UNIVERSAL WISER
PUBLISHER

Research Article

ZnO-Based Memristive Device for Temperature Sensing: Design, Modeling, and Performance Evaluation

Kailasam Rathnakannan[*] , **C. S. Ajai Kumar**

Department of Electrical and Electronics Engineering, College of Engineering, Anna University, Chennai, India
E-mail: krkannan@annauniv.edu

Abstract: This paper presents the design and modeling of a highly sensitive ZnO-based memristive temperature sensor, underpinned by the fundamental physics of memristive behavior. Utilizing a multi-physics simulation tool, the proposed model accurately maps temperature variation contours within the ZnO pyroelectric material, paving the way for its application in temperature sensing. An in-depth exploration of the sensor's electrical properties under varying temperature conditions reveals exceptional sensitivity (8.9 µV/K) and showcases the inherent non-volatile memory switching behavior of the memristor, making it ideally suited for dynamic applications. Moreover, this sensor operates inherently bias-free, functioning as a self-powered solution for emerging fields like the Internet of Things.

Keywords: pyroelectric, temperature, sensor, memristor, ZnO

1. Introduction

Precise and accurate data acquisition is crucial for any system, particularly in smart applications such as the Internet of Things (IoT). Sensors, as the first point of data collection, need to possess critical performance metrics like dynamic capabilities, low power consumption, and high sensitivity. Pyroelectric sensors have found diverse applications in environmental monitoring, condition monitoring of vehicles, gas detection, weather monitoring, and temperature analysis, often contributing to low-power systems and even energy harvesting through their ability to convert temperature fluctuations into electrical signals [1]. However, any sensor, especially wireless ones, faces challenges like leakage power during duty cycles and energy drain due to active-off times, communication, and storage. This is where memristors, with their normally-off and instant-on operation, excel in minimizing leakage power loss. However, the overall power losses in memristor-based systems are influenced by various factors, such as frequency, temperature, and voltage. For instance, resistive (ohmic) losses in ZnO-based memristors have been reported to range from 2% to 5% at frequencies up to 15 Hz for an input voltage range of -2.5 V to $+2.5$ V [2, 3, 4]. These findings highlight the importance of optimized designs to mitigate power losses across a wide range of operating conditions, ensuring the high efficiency and reliability of memristor-based systems. Furthermore, their non-volatile architecture facilitates efficient trade-off computing by reducing off-chip memory access times by 30–70% compared to traditional architectures, depending on workload and memory size [5, 6]. Integrating memristors as sensors can potentially decrease on-chip memory requirements, leading to smaller chip size and lower power dissipation [7, 8]. Beyond memristors, Schottky barrier temperature sensor chips also demonstrate competitive advantages in small chip areas and low power consumption [9, 10]. Schottky-based sensors operate at 2.5

μW to 10 μW and occupy chip sizes of 0.12 mm^2 to 0.25 mm^2 [11]. In contrast, memristor systems show 30–50% power reductions and typically occupy 0.1 mm^2 to 0.2 mm^2 [12, 13].

The significance of memristors lies in their unique relationship between electric charge and magnetic flux linkage, establishing them as the fourth fundamental circuit element besides resistors, inductors, and capacitors [14]. Extensive research has established key circuit-theoretic properties of memristors, including the characteristic hysteresis loop [3]. Non-linear ion drift models indicate that, for DC sources, memristor characteristics exhibit saturation at higher frequencies, resembling resistors. The hysteresis loop is crucial for sensor performance, as it represents an uncompensated error that can affect measurement accuracy. Specifically, the area of the hysteresis loop correlates with the magnitude of errors in output signals. Additionally, electrode size influences the hysteresis behavior, with lower mobility leading to increased memristance and a more pronounced hysteresis loop [13]. Addressing these hysteresis effects is essential for improving the reliability of memristor-based sensors in practical applications.

Zinc oxide (ZnO) nanomaterials have garnered significant attention due to their versatile properties and applications in various fields. Their wide bandgap (3.37 eV) and large exciton binding energy (60 meV) make ZnO an ideal candidate for optoelectronic devices, sensors, and catalysts [15]. Recent studies demonstrate that ZnO-based sensors exhibit remarkable sensitivity and selectivity for various analytes, making them valuable in environmental monitoring and biomedical applications [16, 17]. Furthermore, advancements in fabrication techniques have enabled the development of ZnO nanostructures with tailored morphologies, enhancing their performance [18, 19]. Zinc Oxide (ZnO) stands out as a material possessing valuable properties like semiconductivity, piezoelectricity, and pyroelectricity [20]. Its significant contributions to various applications make it prominent in temperature and gas sensor technology [21]. When subjected to temperature changes, the internal polarization of ZnO generates an electric potential that can be utilized for signal processing. Notably, an increased rate of temperature variation in the ZnO layer enhances the responsivity of the pyroelectric sensor by 10% [22]. Optimizing growth conditions for bulk and epitaxial ZnO films, potentially through doping to achieve a p-type semiconductor and control its electrical stability, can further exploit its semiconductor properties [23, 24]. This study focuses primarily on the memristive behavior of ZnO, exploring its potential as an ambient temperature sensor.

2. Design of sensor model

The sensor proposed in this paper features a zinc oxide (ZnO) active layer sandwiched between top and bottom electrodes. The active region is doped with aluminum and further sandwiched by two electrodes. The ZnO layer sits atop a thermal isolation material to minimize heat loss. When infrared energy strikes the active area, it generates heat and displaces electrons, creating a potential difference between the electrodes. Traditionally, the sensor's top side faces the heat source. However, our design explores the impact of partially or fully covering the active region with the top electrode on the sensor's responsivity.

In the partially covered model, the ZnO directly contacts the heat source, leading to increased heat absorption and higher responsivity compared to the fully covered case. However, a larger exposed area also causes quicker temperature changes within the ZnO layer, ultimately reducing responsivity. To balance these factors, we employ a partially covered electrode with a regular mesh pattern. This mesh design maintains a fixed ratio between the electrode width and bare ZnO surface, ensuring optimal temperature variation and effective top electrode area. Specifically, the top electrode width is 300 nm, occupying half of the 1500 nm cross-section. This width can be further optimized by analyzing the temperature variation in ZnO layers of different thicknesses.

A silicon substrate supports the multilayer sensor. A 130–160 nm silicon nitride (Si$_3$N$_4$) layer deposited on the silicon substrate helps impede thermal conduction. The ZnO active layer, with aluminum doping in a specific region [25], sits between two gold electrodes on top of the Si$_3$N$_4$. Notably, the bottom electrode incorporates a thin chromium layer (9:1 ratio with gold) to act as an adhesive with the ZnO.

Figure 1 shows the two geometrical models designed using COMSOL Multiphysics. Both models have a length of 1400 nm for the fully covered case and 1500 nm for the partially covered case. The ZnO layer thickness varies between 140 nm and 160 nm, as detailed in Table 1. The overall dimensions of the chip are as follows: in the case of a fully covered

electrode, the area is 900 nm × 1400 nm, while for a partially covered electrode, the area is 900 nm × 1500 nm. A regular mesh was used for discretization in both models. For analysis, each model underwent both circuit and heat transfer studies. The circuit analysis employed the Semiconductor study within the Multiphysics tool [26, 27], while the heat transfer study aimed to visualize the temperature variations and gradients within the ZnO layer, thus influencing the sensor's sensitivity. The design of the model considers a temperature range of 0 to 1500 K, which is crucial for the performance evaluation of the proposed system.
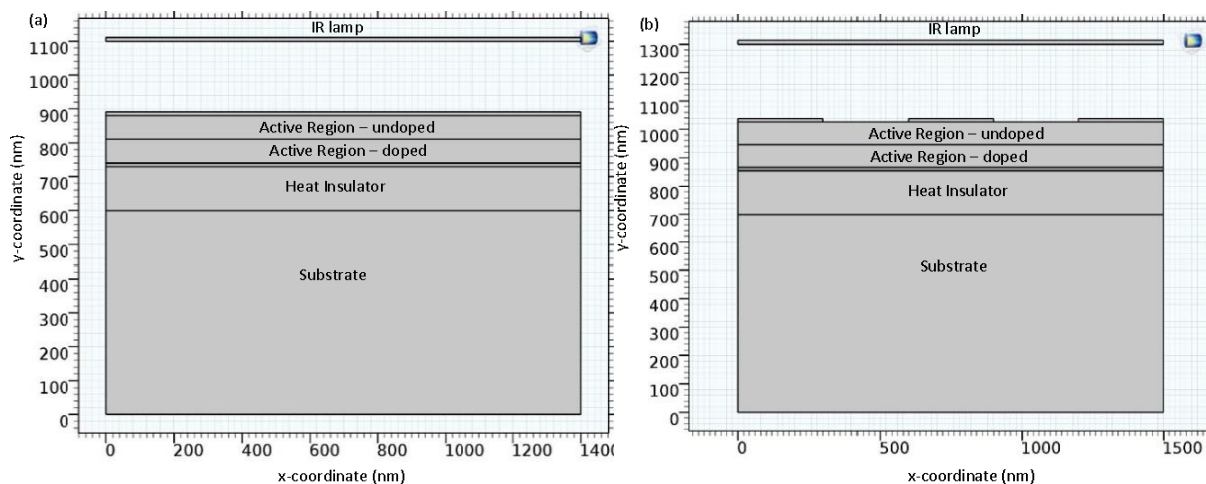

Figure 1. Geometrical structure of the ZnO pyroelectric sensor—(**a**) fully covered electrode model with active region thickness of 140 nm (**b**) partially covered electrode model with active region thickness of 160 nm developed using COMSOL with an IR lamp as heat source on top

Table 1. The dimensions of the fully covered and partially covered electrode models

BLOCK	MATERIAL	FULLY COVERED MODEL HEIGHT (nm)	PARTIALLY COVERED MODEL HEIGHT (nm)
Top electrode	Gold	11	12
Active region (undoped)	ZnO	70	80
Active region (doped)	Al-doped ZnO	70	80
Bottom Adhesive layer	Cromium	1.25	1.5
Bottom electrode	Gold	9.75	10.5
Heat Insulator	Si_3N_4	130	155
Substrate	Silicon	600	700
IR Lamp	-	11	12

3. Results and discussion

The Hysteresis loop is one of the main fingerprint for memristors that clearly depict their characteristics that holds good for any amplitude and frequency of the sinusoidal input. The ZnO based memristive sensor is modelled in the COMSOL Multiphysics and a sinusoidal voltage is given as input. Figure 2 shows the amplitude of the voltage and current as measured between the active region.
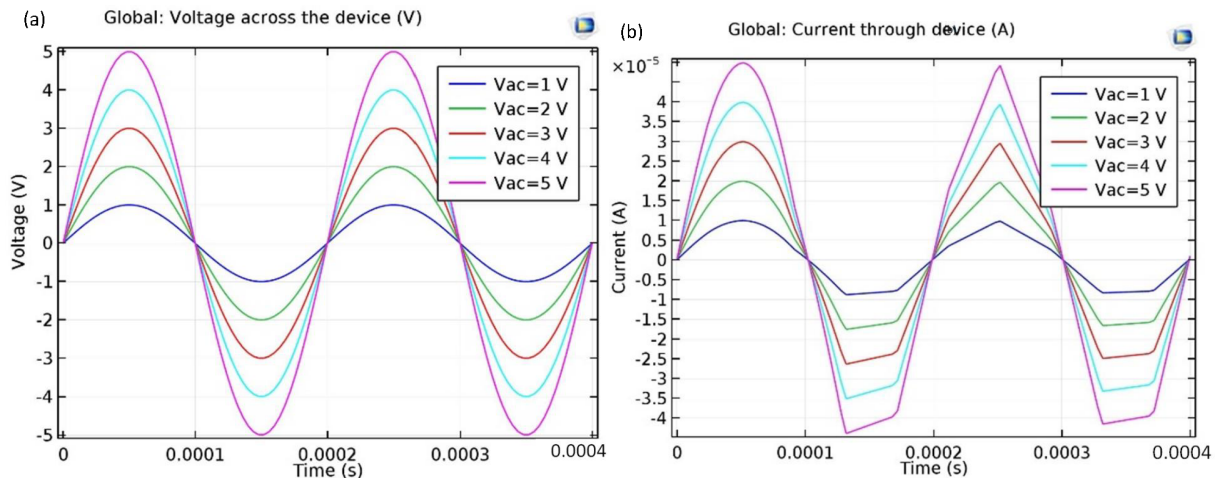
Figure 2. Voltage and Current as measured across the active region sandwiched between the electrodes

The device was subject to range of voltage and frequency combinations and the set of the relative outputs are shown in Figure 3.
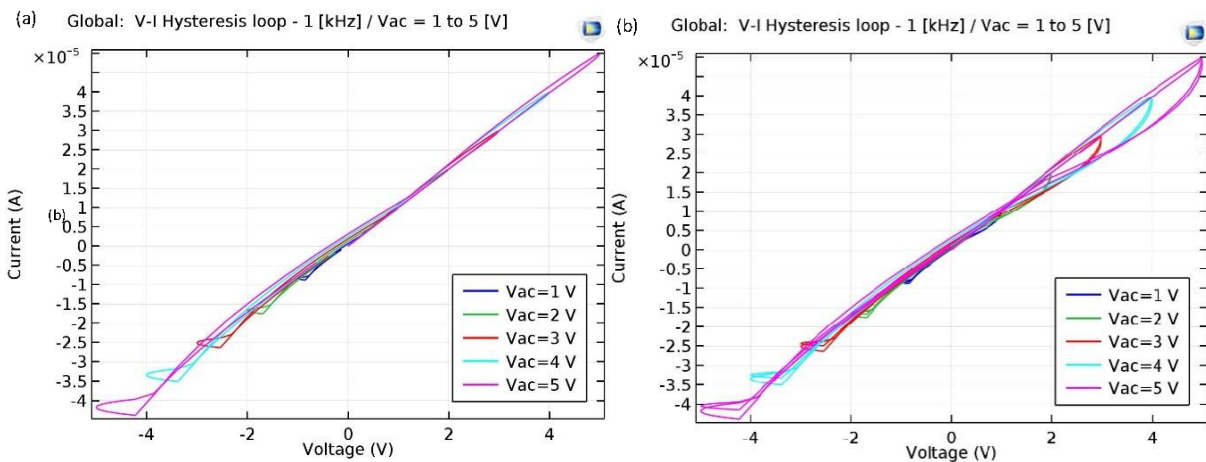

Figure 3. The Hysteresis loop as exhibited on mapping the V-I characteristics (**a**) for an input of 1 kHz and (**b**) 10 kHz under an voltage of 1 to 5 V

The Hysteresis loop tends to become a straight line with the area under the loop falling short at higher voltages and frequencies exhibiting resistance characteristics instead of the memristance effect as inferred. Further the results were narrowed down to 14 kHz frequency range and the observed variations concluded with 14.05 kHz being the critical frequency under 2 V picturizing the pinched hysteresis loop in Figure 4.

Since ZnO exhibits memristive behavior, evidenced by the pinched hysteresis loop observed as shown in Figure 4, its potential as the active component for a temperature sensor is discussed here. We analyze models with both fully covered and partially covered electrode designs. In both cases, an infrared (IR) lamp is placed directly above the model as the heat source. The lamp is set to provide heat radiation at a constant temperature of 493.15 Kelvin throughout the studies.
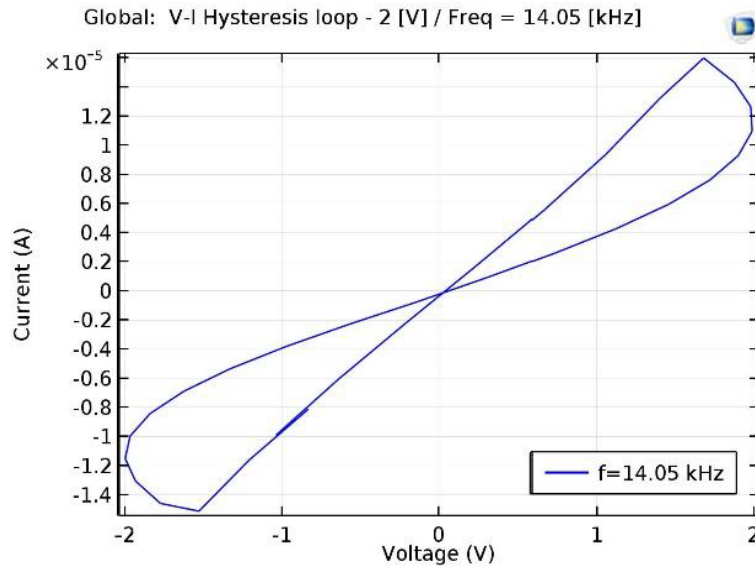
Figure 4. The Hysteresis loop as obtained for the frequency of 14.05 kHz under 2 V

3.1 *Fully covered electrode model*

Figure 5 gives the temperature gradient and the thermal contours developed across the active region as the top region is subject to direct heat from the IR lamp.
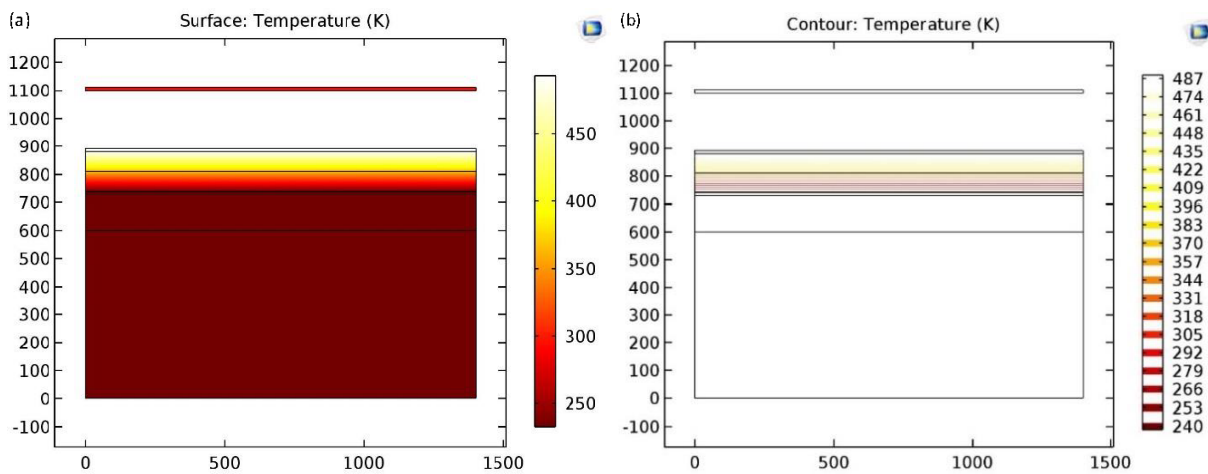

Figure 5. (**a**) Temperature as measured across the active region of the fully covered top electrode sensor model (**b**) the heat contours for the variation in temperature across the active region

The temperature difference across the active region is constant throughout the top region. Hence the temperature gradient or the contour across the region is not variable from time to time.

Figure 6 reveals a crucial finding: the temperature across the active region of the sensor remains uniform throughout the top area. This results in a constant temperature difference, with unchanging contour lines depicting temperature distribution over time. Therefore, the magnitude of the temperature gradient, a key gauge of the device's sensitivity, exhibits minimal variation across the sensor's length.
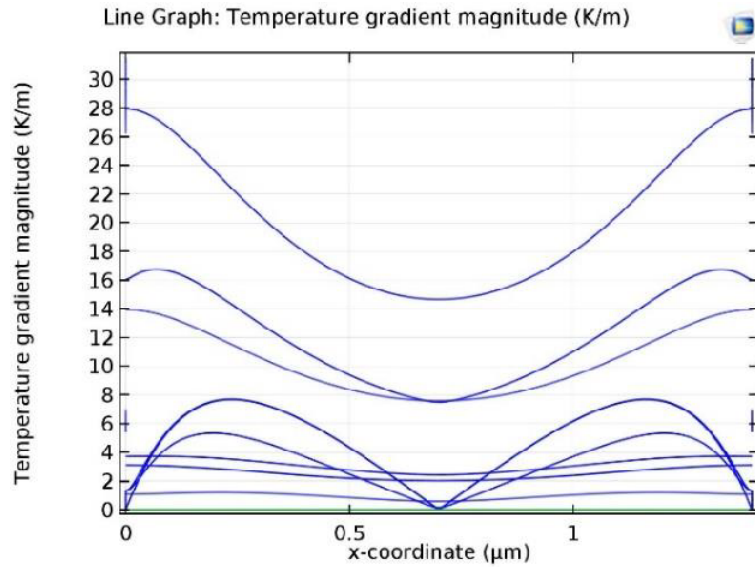
Figure 6. Temperature gradient magnitude measured across the fully covered electrode sensor model length

3.2 *Partially covered electrode model*

Compared to the fully covered electrode, a partially covered model exhibits higher responsivity. This is because it directly exposes the ZnO layer to the heat source. While a larger exposed area fosters greater heat absorption, it also tends to have more dispersed top electrodes. Balancing these factors is crucial in designing the partially covered electrode. The outer regions have a larger exposed ZnO area, while the inner regions benefit from less dispersed top electrodes. Consequently, pyroelectric sensors with partially covered top electrodes experience a higher temperature variation rate in the active region. This effect aligns with observations and plots obtained for the fully covered model. Figure 7 illustrates the temperature measurement and corresponding contours for the partially covered model, clearly showing enhanced heat sensing capabilities in the more exposed ZnO regions.
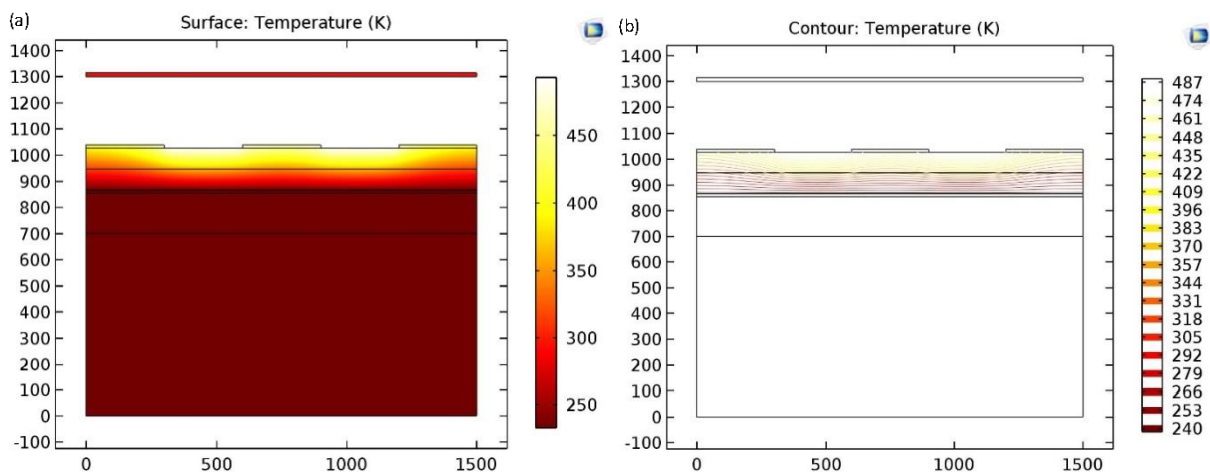

Figure 7. (**a**) Temperature as measured across the active region of the partially covered top electrode sensor model (**b**) heat contours for the variation in temperature across the active region

Figure 8 depicts the temperature gradient magnitude along the device's length. Compared to the fully covered electrode model, the partially covered model exhibits a twofold increase in magnitude, particularly in the exposed porous regions. This enhanced gradient directly translates to improved sensitivity in the utilized active region.
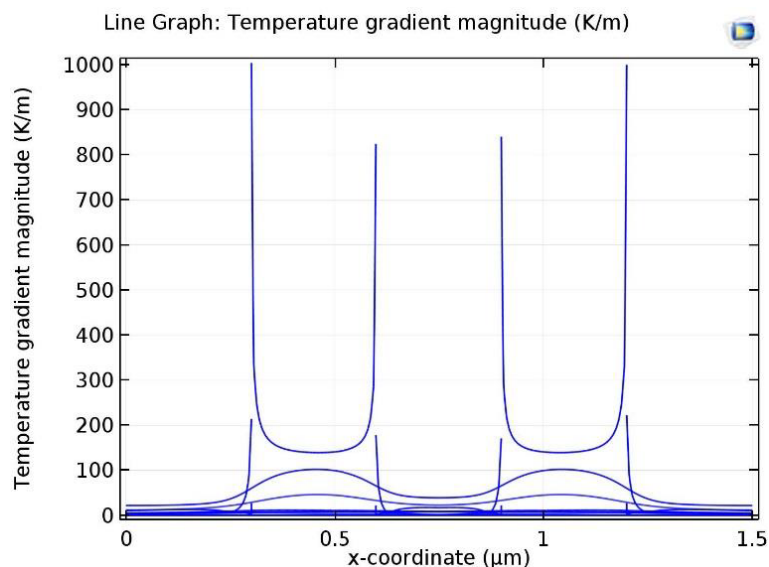

Figure 8. Temperature gradient magnitude measured across the partially covered electrode sensor model

Figure 9 depicts a non-linear line graph revealing the device's voltage response to varying temperatures. We observe a steady voltage increase around 340–380 K and again above 470 K. This highlights the enhanced temperature measurement capability in these ranges, attributed to the device's higher responsivity at these specific temperatures.

Based on this graph, the optimal operating temperature range for the device can be identified within the range of 250–280 K. Additionally, the sensitivity of the device is measured to be around 8.9 µV/K, further indicating its potential for precise temperature sensing within its optimal range. In our study, several nonlinearity indicators of temperature measurement were identified, including deviations from the expected linear response curve of the sensor, the presence of hysteresis effects, and temperature drift over time. These factors can significantly influence the accuracy and reliability of temperature readings, highlighting the importance of careful calibration and characterization in sensor design [28].

Choosing the right memristor for a wireless sensor in an IoT application relies on the insights discussed above. Memristors excel in their operability at low voltage and frequency levels, enabling efficient power management schemes. Additionally, their non-volatile memory, often referred to as a "fingerprint," adds valuable memory capabilities to any wireless sensor node. Based on these advantages, ZnO was chosen as the preferred memristor material, meeting crucial criteria like power consumption, scalability, non-volatility, and, most importantly, the memristive effect itself. Furthermore, the partially covered electrode model, incorporating the memristor's characteristics, emerged as the superior design for the temperature sensor, significantly improving the responsivity of pyroelectric devices.
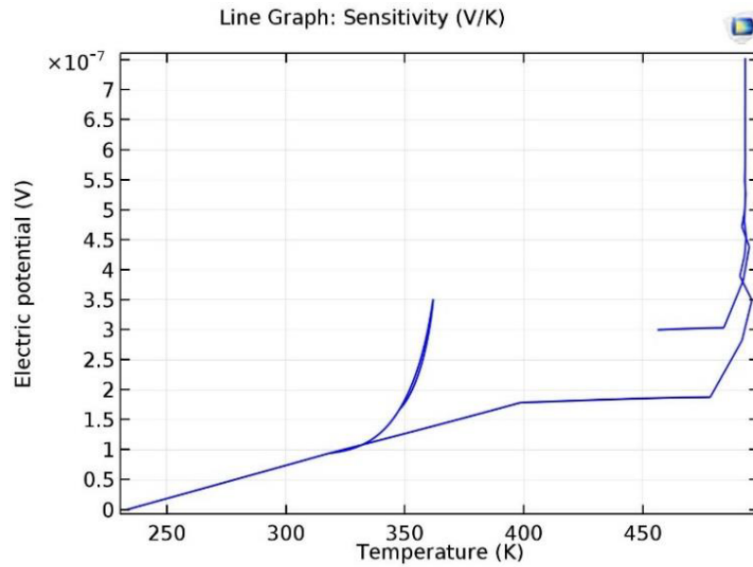
Figure 9. Electric potential developed for the corresponding temperature variations

4. Conclusions

In this study a multi-physics design, modelling and analysis of a ZnO-based temperature sensor that exhibits a unique combination of memristive and pyroelectric properties was reported. This allows the sensor to function as a self-sustaining, low-power device ideal for emulating temperature sensor nodes. Integrating the inherent pyroelectric response of ZnO with its memristive characteristics not only enhances its temperature sensing capabilities but also endows it with non-volatile memory, making it potentially suitable for various IoT applications. Notably, the sensor demonstrates a remarkable sensitivity of around 8.9 µV/K for ambient temperature measurements. Building upon this design, future work can explore the possibilities of creating multi-layered sensing materials, paving the way for the development of versatile multi-purpose sensors.

Acknowledgment

Conflict of interest

The author has no conflicts of interest to declare.

References

[1] C.-C. Hsiao, S.-W. Huang, and R.-C. Chang, "Temperature field analysis for ZnO thin-film pyroelectric devices with partially covered electrode," *Sens. Mater.*, vol. 24, no. 8, pp. 421–441, 2012. https://doi.org/10.18494/SAM.2012.782
[2] S. Paul, P. G. Harris, C. Pal, A. K. Sharma, and A. K. Ray, "Low cost zinc oxide for memristors with high On–Off ratios," *Mater. Lett.*, vol. 130, pp. 40–42, 2014. https://doi.org/10.1016/j.matlet.2014.05.071

[3] L. O. Chua, "Memristor—the missing circuit element," *IEEE Trans. Circ. Syst.*, vol. 18, no. 5, pp. 507–519, 1971. https://ieeexplore.ieee.org/document/1083337

[4] R. Parasuraman and K. Rathnakannan, "Realization of multi-functional features with ZnO nanosheets/p-Si based electronic device for energy harvesting and memristive switching," *Memories*, vol. 2024, p. 100114, 2024. https://doi.org/10.1016/j.memori.2024.100114

[5] K. Nagashima, T. Yanagida, K. Oka, M. Kanai, A. Klamchuen, J. S. Kim, et al., "Intrinsic mechanisms of memristive switching," *Nano Lett.*, vol. 11, no. 5, pp. 2114–2118, 2011. https://doi.org/10.1021/nl200707n

[6] H. Kim, S. P. Adhikari, and M. P. D. Sah, "Three fingerprints of memristor," *IEEE Trans. Circ. Syst. I*, vol. 60-I, no. 11, pp. 3008–3021, 2013. https://doi.org/10.1109/TCSI.2013.2256171

[7] J. Song, Y. Zhang, C. Xu, W. Wu, and Z. L. Wang, "Polar charges induced electric hysteresis of ZnO nano/microwire for fast data storage," *Nano Lett.*, vol. 11, pp. 2829–2834, 2011.

[8] D. B. Strukov, G. S. Snider, D. R. Stewart, and R. S. Williams, "The missing memristor found," *Nature*, vol. 453, pp. 80–83, 2008.

[9] M. Sochacki, A. Kolendo, J. Szmidt, and A. Werbowy, "Properties of Pt/4H-SiC Schottky diodes with interfacial layer at elevated temperatures," *Solid-State Electron.*, vol. 49, no. 4, pp. 585–590, 2005. https://doi.org/10.1016/j.sse.2005.01.015

[10] M. Basov, "Schottky diode temperature sensor for pressure sensor," *Sens. Actuators A*, vol. 331, p. 112930, 2021. https://doi.org/10.1016/j.sna.2021.112930

[11] Ö. F. Yüksel, "Temperature dependence of current—voltage characteristics of Al/p-Si (100) Schottky barrier diodes," *Physica B*, vol. 404, no. 14–15, pp. 1993–1997, 2009. https://doi.org/10.1016/j.physb.2009.03.026

[12] D. Biolek, Z. Biolek, and V. Biolkova, "Interpreting area of pinched memristor hysteresis loop," *Electron. Lett.*, vol. 50, no. 2, pp. 74–75, 2014. https://doi.org/10.1021/nl2011966

[13] K. Rathnakannan, L. N. Alves, J. C. Mendes, and J. C. Pedro, "On the usage of harmonic balance to simulate memristive devices and circuits," in *Proc. 22nd Eur. Conf. Circ. Theory Design*, Trondheim, Norway, Oct. 19, 2015. https://doi.org/10.1109/ECCTD.2015.7300044

[14] H. Abunahla, B. Mohammad, D. Homouz, and C. J. Okelly, "Modeling valance change memristor device: oxide thickness, material type, and temperature effects," *IEEE Trans. Circ. Syst.*, vol. 63-I, no. 12, pp. 2139–2148, 2016. https://doi.org/10.1109/TCSI.2016.2622225

[15] P. Hajara, M. R. Shijeesh, T. P. Rose, and K. J. Saji, "ZnO-based triboelectric nanogenerator and tribotronic transistor for tactile switch and displacement sensor applications," *Sens. Actuators A*, vol. 377, p. 115728, 2024. https://doi.org/10.1016/j.sna.2024.115728

[16] Y. Wang, R. Zhou, H. Cong, G. Chen, Y. Ma, S. Xin, et al., "Weak UV-stimulated synaptic transistors based on precise tuning of gallium-doped indium zinc oxide nanofibers," *Adv. Fiber Mater.*, vol. 5, pp. 1919–1933, 2023. https://doi.org/10.1007/s42765-023-00318-z

[17] S. Keerthana and K. Rathnakannan, "Room temperature operated carbon dioxide sensor based on silver doped zinc oxide/cupric oxide nanoflowers," *Sens. Actuators B*, vol. 378, p. 133181, 2023. https://doi.org/10.1016/j.snb.2022.133181

[18] F. Wang, L. Song, H. Zhang, Y. Meng, L. Luo, Y. Xi, et al., "Advances in electronic materials," *Adv. Electron. Mater.*, vol. 4, no. 1700336, 2018. https://doi.org/10.1002/aelm.201700336

[19] S. Keerthana and K. Rathnakannan, "Hierarchical ZnO/CuO nanostructures for room temperature detection of carbon dioxide," *J. Alloys Compd.*, vol. 897, pp. 162988–162995, 2022.

[20] A. Ukil, "Memristance view of piezoelectricity," *IEEE Sens. J.*, vol. 11, no. 10, pp. 2514–2517, 2011. https://doi.org/10.1109/JSEN.2011.2114878

[21] Y. Sun, X. Yan, X. Zheng, Y. Liu, Y. Zhao, Y. Shen, et al., "High On–Off ratio improvement of ZnO-based forming-free memristor by surface hydrogen annealing," *ACS Appl. Mater. Interfaces*, vol. 7, no. 13, pp. 7382–7388, 2015. https://pubs.acs.org/doi/abs/10.1021/acsami.5b01080

[22] V. Cauda, R. Gazia, S. Porro, S. Stassi, G. Canavese, I. Roppolo, et al., "Nanostructured ZnO materials: synthesis, properties and applications," in *Handbook of Nanomaterials Properties*, B. Bhushan, Ed. Berlin, Heidelberg, Germany: Springer, 2014, pp. 137–177. https://doi.org/10.1007/978-3-642-31107-9_32

[23] A. Janotti and C. G. Van de Walle, "Fundamentals of zinc oxide as a semiconductor," *Rep. Prog. Phys.*, vol. 72, no. 12, p. 29, 2009. https://doi.org/10.1088/0034-4885/72/12/126501

[24] A. Kumar, Y. Rawal, and M. S. Baghini, "Fabrication and characterization of the ZnO-based memristor," in *Proc. 2012 Int. Conf. Emerging Electron.*, Mumbai, India, Dec. 15–17, 2012.

[25] U. M. Al-Saggaf, M. Bettayeb, and S. Djennoune, "Fixed-time synchronization of memristor chaotic systems via a new extended high-gain observer," *Eur. J. Control*, vol. 63, pp. 164–175, 2022. https://doi.org/10.1016/j.ejcon.2021.10.002

[26] Y. Cohen and A. Ya'akobovitz, "Comparative study on modeling approaches of V-shaped MEMS temperature sensors," *IEEE Trans. Instrum. Meas.*, vol. 68, no. 10, pp. 3766–3775, 2018. https://doi.org/10.1109/TIM.2018.2879144

[27] R. Parasuraman and K. Rathnakannan, "Thermal analysis in 3-D simulation of thin-film $ZnO/MoS_2/Si$ solar cells," *Multiscale Multidiscip. Model. Exp. Des.*, vol. 7, pp. 3815–3826, 2024. https://doi.org/10.1007/s41939-024-00440-4

[28] R. A. John, N. Shah, S. K. Vishwanath, S. E. Ng, B. Febriansyah, M. Jagadeeswararao, et al., "Halide perovskite memristors as flexible and reconfigurable physical unclonable functions," *Nat. Commun.*, vol. 12, p. 3681, 2021.